Desalination and Water Treatment
www.deswater.com

doi: 10.5004/dwt.2021.27043

221 (2021) 260–269
May

Arsenite adsorption on biochar-based nano copper oxide composites using Mediterranean cypress cones: equilibrium, kinetic and thermodynamic studies

Imad Hamadneh[a,*], Ahmed Al-Mobydeen[b], Fayza Hannoon[a], Afnan Abu Jaber[a], Rula Albuqain[c], Shorouq Alsotari[c], Ammar H. Al-Dujaili[d]

[a]*Department of Chemistry, Faculty of Science, University of Jordan, Amman 11942, Jordan, Tel. +962 775500003; email: i.hamadneh@ju.edu.jo (I. Hamadneh), Tel. +962798408852; email: fayza96_7annoon@yahoo.com (F. Hannoon), Tel. +962775904574; email: afnanabujaber44@yahoo.com (A.A. Jaber)*
[b]*Department of Chemistry, Faculty of Science, Jerash University, Jerash 26150, Jordan, Tel. +962798962089; email: ahmeddd_mob@yahoo.com*
[c]*Cell Therapy Center (CTC), The University of Jordan, Amman 11942, Jordan, Tel. +962798738536; email: buqaien@yahoo.com (R. Albuqain), Tel. +962796605076; email: shalsotari@gmail.com (S. Alsotari)*
[d]*Hamdi Mango Center for Scientific Research, University of Jordan, Amman, P.O. Box: 11942, Jordan, Tel. +962796629774; email: ah.aldujaili@gmail.com*

Received 15 August 2020; Accepted 14 January 2021

ABSTRACT

The removal of arsenite using biochar (BC) and biochar-CuO nanocomposite (BC-CuO-NC) from cypress cones biomass was systematically investigated. The copper oxide (CuO) nanoparticles (NP's) were synthesized using aqueous cypress cones extract. The BC was obtained by the pyrolysis of cypress cones biomass at 550°C and then impregnated with CuO-NP's to produce BC-CuO-NC. Arsenite adsorption into BC and BC-CuO-NC was studied using the batch technique at different pH, contact time, adsorbent dose, and temperature conditions. BC-CuO-NC demonstrated better adsorption efficiency than BC to 5–6 pH arsenite with a 55.58% removal percentage and a 10 min balance period. Compared with the Dubinin–Radushkevich isotherm equation, the Langmuir and Freundlich isotherm equations fit well with the experimental results. According to the Langmuir model, the saturated adsorption capacity of BC and BC-CuO-NC for arsenite can reach 22.831 and 36.765 mg/g, respectively. Kinetic studies have shown that the adsorption arsenite on BC and BC-CuO-NC was defined in pseudo-second-order. The determined thermodynamic parameters of the adsorption cycle were spontaneous, exothermic, and the random increase was observed.

Keywords: Biosorption; Biochar; Arsenite; Nanocomposite; Mediterranean cypress cones; Isotherm

1. Introduction

The rapidly deteriorating water quality in many of the water resources and increasingly stringent legislation on the purity of drinking water has created a growing interest in the decontamination of water, wastewaters, and polluted trade effluents using different adsorbents in either crude or modified forms [1]. Inorganic trivalent arsenic (As(III), arsenite) exists as uncharged (H_3AsO_3) or anionic species ($H_2AsO_3^-$), ($HAsO_3^{2-}$), and (AsO_3^{3-}) [2–4]. It is more toxic than organic ones, and As(III) is more toxic than As(V) for human beings and animals [5,6]. Around 200 million people worldwide are exposed to an arsenic concentration in drinking water that exceeds the recommended limit of 10 ppb as set out in the guidelines of the

* Corresponding author.

World Health Organization (WHO) [7]. The excess intake of arsenic may cause health problems, including cancers of the lungs, kidneys, bladder, skin, liver, prostate, and other diseases [8,9]. Due to natural and human activities such as arsenic pesticides, irrigation and oxidation fertilizers of volatile arsine in the air [10], dust from the burning of fossil fuel, as well as the disposal of industrial, municipal, and animal waste [11]. Among the available methods for water treatment, adsorption has emerged as an option for developing an economical and eco-friendly process for removing arsenic from wastewater [12–15]. Biochar from agricultural waste, kitchen waste, and sewage sludge as an adsorbent was used to remove the arsenite [16–20].

Biochar as a low-cost adsorbent, sustainable, environmental friendly, easy production process, unique properties (pore volume, pore size, high surface area, pH, electrical conductivity (EC), cation exchange capacity (CEC) and surface functional groups) offers an attractive and inexpensive option for the removal of contaminants from water [13]. The addition of metal oxide nanoparticles via impregnation improves the removal efficiency of the anionic pollutants from water by increasing the positive surface charged of biochar [21]. As an example, a reusable Mg–Fe–Cl layered double hydroxide was also used as a high efficiency of adsorption of As(III) from aqueous solution [22].

The purposes of this work were to: (1) the preparation of copper oxide (CuO) nanoparticles (NP's) using aqueous cypress cones extract and the production of biochar by pyrolysis process and then impregnated with CuO-NP's to produce biochar-CuO nanocomposites and (2) using both biochar and biochar-CuO nanocomposites as an adsorbent for the removal by a batch method of arsenite species from aqueous solutions. Various variables have been investigated, such as adsorbent dosage, pH, contact time, and temperature. Furthermore, the isotherms of thermodynamics, kinetics, and adsorption were studied at various temperatures.

2. Experimental

2.1. Sample preparation

2.1.1. Plant extracts preparation

A 50 g of Mediterranean cypress (*Cupressus sempervirens*) cones powder were boiled in 500 mL of deionized water for 10 min under vigorous stirring, then the mixture was cooled to room temperature and filtered through using suction filtration to remove the cones particles (biomass), and the clear extract of Mediterranean cypress cone obtained (pH equal to 5.2 and conductivity equal to 91.1 μs^{-1}) was refrigerated at 4°C for further use for the synthesis of nanoparticles.

2.1.2. Synthesis of CuO-NP's

Copper oxide nanoparticles (CuO-NP's) was prepared by adding 50 mL of 0.10 M copper(II) acetate solution to 275 mL of cypress cones extract for 10 min under vigorous stirring (600 rpm) and ambient temperature. The brown precipitate was formed as an indicator of metal complex formation. Then, the brown slurry was filtered, centrifuged for 15 min at 6,000 rpm, dried overnight in the oven at 60°C, and calcined at 750°C. The color of the powder was changed to black.

2.1.3. Synthesis of biochar and biochar-CuO nanocomposite

Biochar (BC) was prepared from cypress cones biomass (raw) where dried crushed biomass (100 g) was wrapped with aluminum foil and placed in a muffle furnace at 550°C for 2 h and then cooled to room temperature. Biochar-CuO nanocomposite (BC-CuO-NC) was prepared via impregnation method where 10 g of prepared biochar was added to 0.5 g of CuO-NP's dissolved in 100 mL H_2O under sonication for half an hour. The mixture was stirred at room temperature for 12 h, fluxed for 1 h, filtrated, and centrifuged for 15 min at 6,000 rpm. The resultant was washed by deionized water, and finally, the BC-CuO-NC was dried in the oven at 110°C overnight.

2.2. Adsorption experiments

Arsenite As(III) adsorption on BC and BC-CuO-NC samples was carried out using batch techniques at a constant temperature. In a typical adsorption run, 0.5 g of BC or BC-CuO-NC was equilibrated with 50.0 mL arsenite solution in a stopper 100 mL Erlenmeyer flask in a thermostatic water bath shaking at a constant temperature for 24 h. The arsenite solution was separated from the adsorbent by centrifugation at 6,000 rpm for 15 min and filtration with a 0.22 μm syringe filter. The supernatant was subsequently analyzed for a residual concentration of As(III) ions using inductively coupled plasma-optical emission spectroscopy (ICP-OES). The amounts of arsenite and the percentage removal of adsorption (%*R*) adsorbed by the BC or BC-CuO-NC were calculated using the following equations:

$$q_e = \frac{\left(C_0 - C_e\right)V}{m} \tag{1}$$

$$\%R = \frac{\left(C_0 - C_e\right)}{C_0} \times 100 \tag{2}$$

where q_e (mg/g) is the amount of arsenite adsorbed by BC or BC-CuO-NC, C_0 and C_e (mg/L) are the initial and equilibrium concentration of arsenite, respectively, V (L) the initial volume of arsenite solution and m (g) the weight of the adsorbent.

2.3. Characterization

BC and BC-CuO-NC aqueous solutions were prepared; the pH was measured with a Metrohm pH Meter. EC was determined by (Eutech Con 2700, Singapore) instrument. Fourier-transform infrared spectroscopy (FTIR) spectra of samples were recorded using Thermo-Nicolet NEXUS 670 FTIR spectrophotometer (Waltham, MA USA 02451). Elemental analyses of the samples were done by using EuroVector EA3000 Elemental Analyzer (Italy). The thermal gravimetric analysis (TGA) of the dried samples was studied using NETZSCH STA 409 PC/PG Thermal Analyzer (Germany) in the temperature range (25°C–900°C), at a heating

rate of 20°C/min. The samples were analyzed by an X-ray powder diffractometer with CuKα radiation (λ = 1.5418 Å) using the X'Pert Pro X-ray diffraction (XRD) method of PANalytical (Eindhoven, Netherlands) at 45 kV and 40 mA with a phase of 0.02 alike over the 10–90 range. The sample texture and surface morphology were examined using the FEI VERSA-3D model attached with the STEM detector.

The shaking of samples was performed using a thermostat fitted shaker GFL-1083.The specific surface area determined by Brunauer–Emmett–Teller (BET) equation using NOVA 2200E Surface Area and Pore Size Analyzer (Quantachrome Corporation, Boynton Beach, Florida, USA). The arsenite concentration was estimated by inductively coupled plasma-optical emission spectrophotometer (ICP-OES) model Quantima – GBC Scientific.

The physical and chemical parameters such as yield%, ash contents, moisture%, pH, and pH zero-point charge (pH_{ZPC}) were studied using procedures in El Hanandeh et al. [21].

3. Results and discussion

3.1. Characterization of adsorbent

FTIR spectra of biomass (raw), BC, CuO-NP's and BC-CuO-NC are shown in Fig. 1. The bands appeared at 868 and 720 cm^{-1} due to aromatic C–H deformation modes, 1,014 C–O stretching of C–OH groups, 1,600 cm^{-1} is due to C=O stretching. This peak comprises a variety of C=O containing functional groups, including ketones, carboxylic acids esters, and anhydrides, 1,399 cm^{-1} C–C stretching vibration in the aromatic ring, 2,934 cm^{-1} due to C–H aromatic stretching vibration, 2,800–3,600 cm^{-1} O–H stretching of water molecules were adsorbed on the surface, all the above-mentioned bands are found in all figures except for CuO-NP's. The FTIR spectra of BC-CuO-NC has both bands in CuO and BC identify some important functional groups in addition where the absorption bands located at 443, 477, 606, 621, 1,043 and 1,105 cm^{-1} were assigned to the vibration of the Cu–O [23,24]. Peaks appeared at 1,410 and 1,520 cm^{-1}, corresponding to the C–O stretching of carboxylate ion bond to the CuO-NP's as a bidentate ligand.

The thermal properties of biomass, biochar, and BC-CuO-NC were carried out using TGA as shown in Fig. 2. Biomass decomposition developed in two stages, an initial mass loss of around 4% between the temperatures of 60°C and 220°C due to moisture evaporation. The second stage occurred at 350°C–650°C (70%) due to organic decomposition (the residue 25.35% and a net mass loss of 74.65%). BC decomposition showed a simple drop of 5.4% even the temperature was above 550°C. BC-CuO-NC decomposition occurred between 350°C–600°C with a mass loss of 8% [25].

Fig. 3 shows the XRD pattern for CuO-NP's, BC and BC-CuO-NC, for CuO-NP's it is shown that the peaks 32.5°, 35.5°, 46.2°, 48.7°, 53.5°, 58.3°, 61.5°, 65.8°, 66.2°, 68.0°, 72.4°, 75.0° and 75.2° are belonging to monoclinic structure with a space group of C2/c. The lattice parameters a_o, b_o and c_o are 4.69 Å, 3.43 Å and 5.14 Å with precision less than ±0.01, where α, γ are 90.00°, the β is 99.53°. This result is matched with the standard reference (ICDD# 00-001-1117). XRD pattern for BC showed a broad peak appeared at 10°–35° as an indication of amorphous behavior, and the peaks appeared at the 2θ value 16°, 22°, 26°, 28°, 38°, 43°, 44°, 47°, 48°, and 49° are an indication of crystalline behavior for BC. However, after the impregnation with CuO-NP's, the peaks for both systems existed as an indication of BC-CuO-NC formation.

The scanning electron micrograph for BC and BC-CuO-NC showed a plate-like structure with an irregular shape appeared. The texture has a high porosity where the gaps and voids exist with an average pore size of 5–15 um (Fig. 4). Figs. 4a and b are looking the same under the secondary electron detector, where the using backscattered mode, the composite showed a bright area scattered on the surface of the composite, which is due to the CuO-NP's adhered to the biochar surface.

BET was used to calculate the total volume of pore from the close uptake of saturation (P/P_0 = 0.99). The Barrett–Joyner–Halenda method measured the mesopore length, mesopore surface area, and pore size distribution. The BET surface area, total pore volume (V_{total}), average pore diameter (r_{BET}), and pore structures of BC and BC-CuO-NC are listed in Table 1. Results showed that there is a decrease in the surface area (SA), total pore volume (V_{total}), and average pore diameter (r_{BET}) with impregnation of CuO-NP's

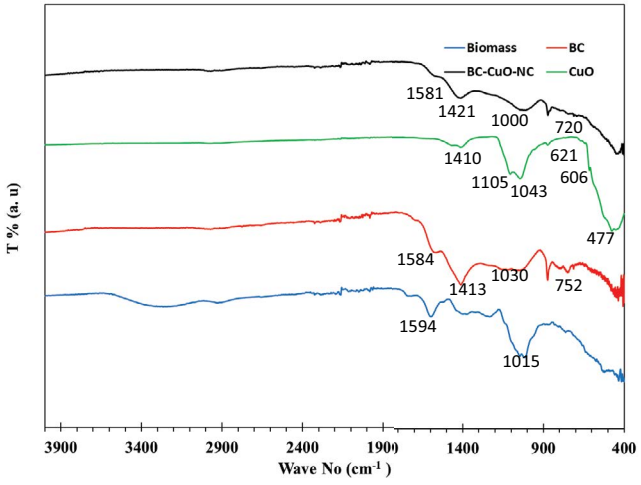

Fig. 1. FTIR spectrum for biomass, BC, CuO-NP's, and BC-CuO-NC.

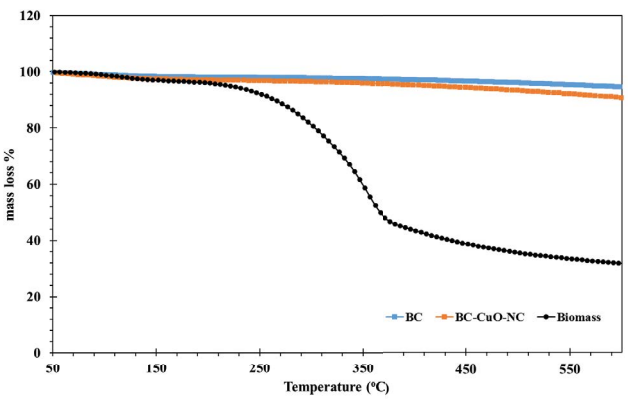

Fig. 2. TG thermogram of biomass, BC, and BC-CuO-NC.

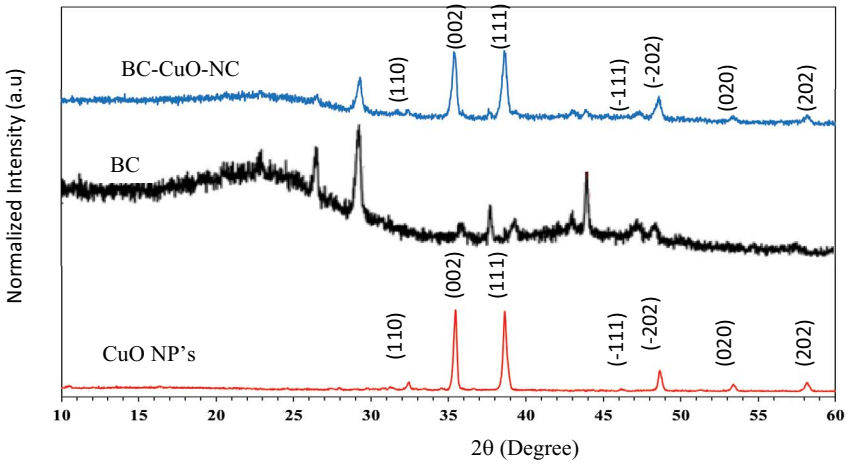

Fig. 3. X-ray diffractogram of CuO-NP's, BC, and BC-CuO-NC, the peaks labeled (hkl) belong to CuO.

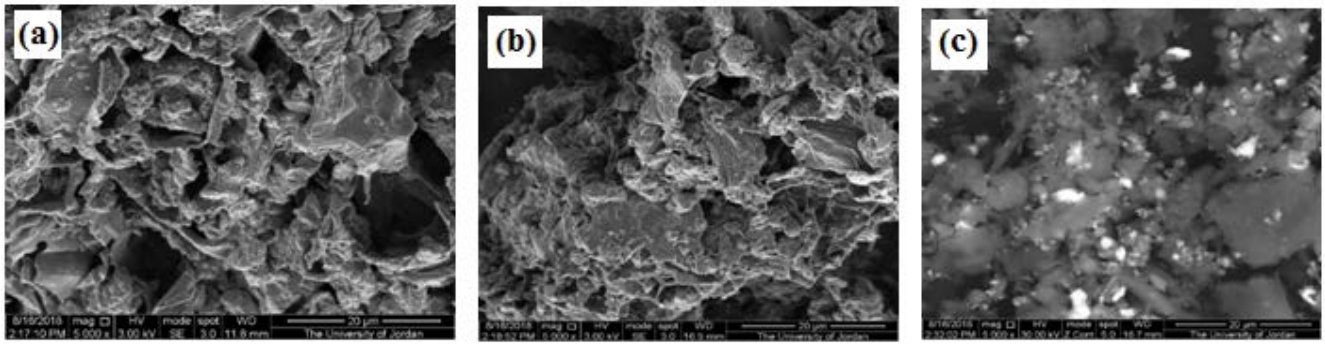

Fig. 4. Scanning electron micrograph in secondary electron mode for (a) BC, (b) BC-CuO-NC, and (c) BC-CuO-NC in back-scattered mode.

to the BC surface to form BC-CuO-NC due to blockage of bores by CuO-NP's. The pore structures are mesoporous for BC and BC-CuO-NC. External in mesopores surface area is equal to 8.985 m^2/g and can be calculated from the difference between $SA_{BET} - A_{meso}$ and non-meso volume is equal to 0.315 and can be calculated from the difference between $V_{total} - V_{meso}$ [26].

CEC is a measure of how many cations can be retained by BC and BC-CuO-NC surfaces. The calculation was carried out by measuring the adsorption of bis(ethylenediamine) copper(II) complex $[Cu(en)_2]^{2+}$ on BC or BC-CuO-NC. The method was clearly explained in the literature [27]. The CEC results are 83.166 (cmolc/kg) for BC and 82,351 (cmolc/kg) for BC-CuO-NC. Decreasing in CEC means that the negative charge on the BC-CuO surface decreased with an increase in positive charge [28].

The physicochemical properties of BC and BC-CuO-NC including the yield, moisture and ash contents, specific surface area, pH, pH_{ZPC}, and elemental analysis were mentioned are consistent with the impregnation of CuO-NP's to the BC (Table 2). The increase of the H/C ratio in BC-CuO-NC over BC indicates good preservation of the original contents in the BC-CuO-NC with lower degree aromaticity. The polarity index (O+N)/C ratios increased to 0.416% for BC-CuO-NC is an indication of the surface polar functional groups and leads to electrostatic attraction enhancement towards the removal of As(III) via the positively charged BC-CuO-NC. H/C and O/C elemental ratios can be used to predict the structural stability of the BC-CuO-NC at the function of time [29].

Table 1
BET surface area, total pore volume (V_{total}), and average pore diameter

Sample	BC	BC-CuO-NC
SA_{BET} (m^2/g)	42.494	15.006
SA_{meso} (m^2/g)	33.509	10.903
V_{total} (cm^3/g)	0.042	0.038
V_{meso} (cm^3/g)	0.039	0.008
r_{BET} (nm)	3.967	10.093
D_{ap} (nm)	2.54	1.34

3.2. Biosorption experiments

The effects of adsorbent dose, contact time, initial pH, and adsorbent temperature were investigated. The effect of adsorbent dose on arsenite removal was studied by taking

50 mL of 59 ppm of arsenite containing 0.10–0.50 g/50 mL of BC or BC-CuO-NC and being shacked in a water bath at 25°C for 24 h and pH 6.5.

3.2.1. Effect of adsorbent dosage of BC and BC-CuO-NC

The effect of BC and BC-CuO-NC dosages on the percentage removal (%*R*) and the adsorption quantity q_e (mg/g) As(III) ions at 25°C is presented in Fig. 5. The %*R* of As(III) ions increased with the increase of the adsorbent dose from 0.1 to 0.5 g per 50 mL solution and was found to be 30.6% and 44.4% at the appropriate dose of 0.5 g/59 mL for BC and BC-CuO-NC, respectively.

The availability of active sites on adsorbents' surface helped arsenite molecules reach the adsorption sites more easily [21,30]. Further increases in the adsorbent dosage did not affect arsenite removal. It appears that the impregnation of BC with CuO-NP's to produce BC-CuO-NC increases the sorption of arsenite. The corresponding adsorption capacity (q_e) of arsenite decreased with increasing the adsorbent dose. Above this dose (0.5 g BC and BC-CuO-NC per 50 mL solution), the percent adsorption of arsenite increases very slowly almost attains equilibrium.

Table 2
The yield%, ash%, moisture%, pH values, pH_{ZPC}, chemical compositions and atomic ratios of BC and BC-CuO-NC produced from cypress cones biomass at 550°C pyrolytic temperature

Sample	BC	BC-CuO-NC
Yield%	30.7	100
Ash%	11.7	19.4
Moisture%	0.25	3.72
pH	9.93	8.48
pH_{ZPC}	8.76	9.44
C%	76.0	68.4
H%	2.25	2.22
N%	1.43	1.01
O%	20.3	28.4
H/C	0.030	0.033
N/C	0.019	0.015
O/C	0.267	0.416
(O+N)/C	0.004	0.416

3.2.2. Effect of pH and pH_{ZPC} of BC and BC-CuO-NCs

Fig. 6 represents the effect of varying pH on As(III)'s removal efficiency by BC and BC-CuO-NC from aqueous solution. The maximum As(III) adsorption for BC was found at pH = 7.1, where the BC-CuO-NC increase in adsorption efficiency as the pH increased. The surface load on the BC and BC-CuO-NC is related to their zero-point (pH_{ZPC}) pH charge. The BC pH_{ZPC} (8.76) was lower than the BC pH (9.93), indicating richness in negative charges on the biochar's surface. In contrast, the pH_{ZPC} of the BC-CuO-NC (9.44) was higher than the pH of the BC-CuO-NC (8.48), indicating richness in positive charges on the BC-CuO-NC surface. The adsorption of As(III) on BC and BC-CuO-NC was dependent on the arsenic valence and the pH of the solution. At pH levels normally present in natural conditions, As(III) exists as the undissociated acid H_3AsO_3; in alkaline conditions (pH > 9), as $H_2AsO_3^-$; and at pH higher than 12

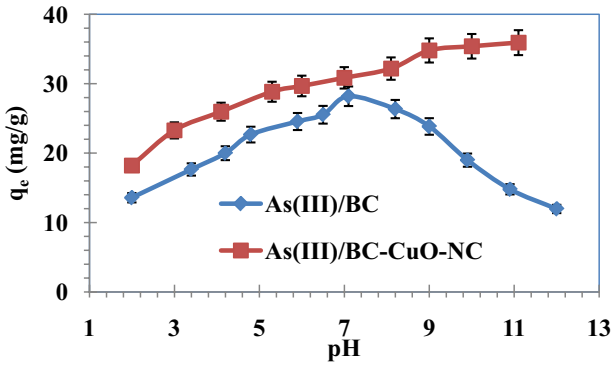

Fig. 6. Effect of pH on arsenite removal by BC and BC-CuO-NC. Condition: different concentrations; adsorption dosage of 0.35 g/50 mL; *T* = 25°C.

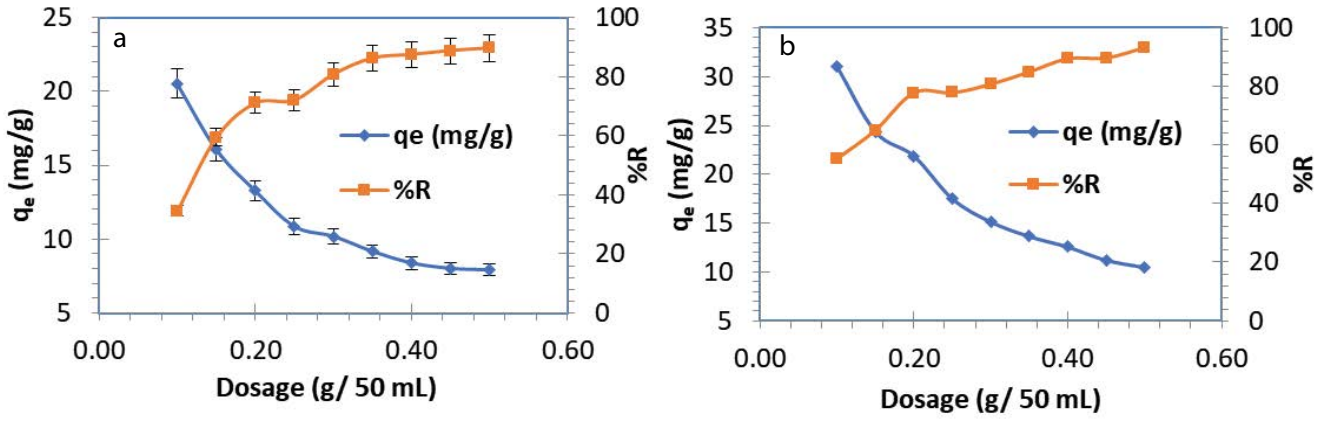

Fig. 5. Effect of adsorbent dose (g/50 mL solution) on adsorption of As(III) onto adsorbent (a) BC and (b) BC-CuO-NC. Initial concentration of arsenite 59 mg/L; agitation speed 150 rpm and 25°C.

as $HAsO_3^{2-}$. BC's surface was negatively charged up to its pH_{ZPC} value of 8.76, with the pH increase up to this value, an increase in As(III) adsorption capability was observed primarily due to the van der Waals interaction between the neutral arsenic species and the BC surface. A strong decrease in adsorption was observed above pH 8.76 as a result of increased electrostatic repulsion between BC's negative surface sites and the dominant-negative arsenic species of $H_2AsO_3^-$ and $HAsO_3^{2-}$. There's strong agreement with these findings by the study of Liang et al. [31].

3.2.3. Effect of contact time and adsorption kinetics

The contact time for arsenite on the BC and BC-CuO-NC was calculated from 5 to 180 min at a fixed arsenite concentration of 77 mg/L, a dosage of adsorbent of 0.35 g/50 mL solution, agitation speed 150 rpm, temperature 25°C (Fig. 7). Results showed that arsenite adsorption on BC and BC-CuO-NC is accompanied by a two-stage kinetic behavior: arsenite adsorption initially increased significantly up to the first 10 min, followed by a second stage with a much lower adsorption rate at the initial stage of 60–180 min, with time, the adsorption curve rises sharply, indicating that arsenite adsorption rates are very high and that there are plenty of accessible sites. The adsorption reaches a maximum, 55.58% with a capacity of 22.514 mg/g at 60 min for BC, and reaches a maximum of 87.52% with a capacity of 34.338 mg/g at 60 min, after that remains unchanged with further time. Hence, the optimum contact time was selected as 60 min for further experiments. The arsenite adsorption rate is high at the beginning of the experiment because initially the adsorption sites are more available and arsenite ions are easily adsorbed on these sites until all adsorption sites reached saturation.

The adsorption kinetics is important data to understand the adsorption mechanism and evaluate the performance of the adsorbents. Three kinetic models, including the Lagergren pseudo-first-order, pseudo-second-order, and intraparticle diffusion model, were applied for the experimental data to predict the adsorption kinetics [30,32].

Adsorption kinetics is one of the critical components to be responsible for adsorption diffusion efficiency.

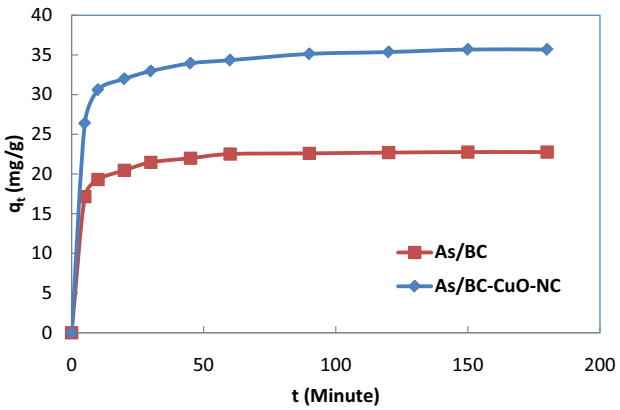

Fig. 7. Effect of contact time for the removal of arsenite by BC and BC-CuO-NC. Dosage = 0.35 g; arsenite conc. = 77 mg/L, 77 mg/L; contact time from 5 to 180 min.

The kinetic parameters are useful for predicting the adsorption rate, which gives valuable information for process design and modeling. These three models were tested to fit the experimental data obtained from arsenite biosorption as shown in Eqs. (3)–(5).

Pseudo-first-order model [33]:

$$q_t = q_e\left(1 - e^{-k_1 t}\right) \tag{3}$$

Pseudo-second-order model [34]:

$$q_t = \frac{k_2 q_e^2 t}{1 + k_2 q_e t} \tag{4}$$

Intraparticle diffusion equation [35]:

$$q_t = k_{id} t^{0.5} + C \tag{5}$$

where q_t is the sum of arsenite adsorbed at time t (mg/g), k_1 is the pseudo-first-order constant (min^{-1}), k_2 is the pseudo-second-order adsorption equilibrium constant (g/mg min), k_{id} is the constant intraparticle diffusion rate (mg/g min) and C is constant.

The kinetic data obtained from the nonlinear regression analysis fitting for BC and BC-CuO-NC together with R^2, χ^2 and $F_{error\%}$ are shown in Fig. 8 and Table 3. The values of R^2 were low and χ^2 and $F_{error\%}$ were high, and the calculated q_e value does not agree with the experimental value that the adsorption of arsenite onto BC and BC-CuO-NC is not first-order kinetics. These results agree with the results reported by Mohammed et al. [36]. Results in Table 3 show that the values of R^2 are very high, and χ^2 and $F_{error\%}$ were very low, and the experimental q_e value with a good agreement with the calculated value. This result indicates that arsenite's adsorption onto BC and BC-CuO-NC follows the pseudo-second-order kinetics [32]. For the arsenite adsorption intraparticle diffusion model on BC and BC-CuO-NC, if the line passed through the center, then the intraparticle diffusion was the only rate-limiting operation. Otherwise, besides intraparticle diffusion, the rate-limiting cycle included other mechanisms [37]. The line did not pass through the origin, which was not the only rate-controlling step in the adsorption process that indicated intraparticle diffusion.

3.2.4. Adsorption isotherm models

Adsorption equilibria provide physiochemical data for evaluating the applicability of the adsorption process. In this work, three models (Langmuir, Freundlich, and Dubinin–Radushkevich) were used to describe the relationship between the amount of arsenite adsorbed and its equilibrium concentration for all BC and BC-CuO-NC adsorbents as shown in Eqs. (6)–(8).

Langmuir isotherm model [38]:

$$q_e = \frac{q_{max} K_L C_e}{1 + K_L C_e} \tag{6}$$

Freundlich isotherm model [39]:

$$q_e = K_F C_e^{1/n} \tag{7}$$

Dubinin–Radushkevich (D–R) isotherm model [40]:

$$q_e = q_{\max} \exp\left(-\beta \left[RT \ln\left(1 + \frac{1}{C_e} \right) \right]^2 \right) = q_{\max} \exp\left(-\beta \varepsilon^2 \right) \quad (8)$$

where q_e is the uptake of arsenite per unit weight of BC and BC-CuO-NC (mg/g), $q_{\max}$ is the maximum uptake of arsenite (mg/g), K_L is the Langmuir constant (L/mg) and related to the adsorption energy, C_e is the phenol (mg/L) equilibrium concentration, K_F is the Freundlich constant [mg g^{-1} (L $mg^{-1})^{1/n}$] denoting adsorption capacity, n is the empirical constant, indicating adsorption intensity, ε the Polanyi potential equal to $RT\ln(1 + 1/C_e)$, β, R, and T suggests a constant relative to adsorption energy, gas constant (8.314 J/mol K), and temperature (K), respectively, E (kJ/mol) is the mean free adsorption energy per adsorbent molecule when transferred from infinity to the solid surface in the solution.

The equilibrium data for arsenite adsorption using BC and BC-CuO-NC as adsorbents were fitted with the equations Langmuir, Freundlich, and D–R (Fig. 9). Table 4 summarizes the data of the fitted models at 25°C along with R^2, χ^2 and $F_{error\%}$.

From Table 4 it can be seen that the regression coefficient (R^2, χ^2 and $F_{error\%}$) of the Langmuir and Freundlich equations ((R^2 > 0.9778, χ^2 < 0.195 and $F_{error\%}$ < 5.96) is more fitted when compared with that of the D–R equation (R^2 > 0.7593, χ^2 < 1.539 and $F_{error\%}$ < 17.29) implying that the adsorption of arsenite onto BC and BC-CuO-NC models show a complex mechanism involving both monolayer and multilayer on heterogeneous surface conditions. The data in Table 5 indicate that the maximum adsorption capacities $q_{\max}$ estimated using the Langmuir isotherm model for arsenite was 22.831 and 36.765 mg/g onto BC and BC-CuO-NC, respectively.

Langmuir isotherm can be characterized by a dimensionless constant called the separation factor (R_L) equation. The value of R_L indicates the shape of the isotherm to be either linear (R_L = 1), unfavorable (R_L > 1), favorable (0 < R_L < 1), or irreversible (R_L = 0), In this work, the R_L values were between 0 and 1 (0.542 and 0.642) (Table 5) for arsenite adsorption onto BC and BC-CuO-NC, respectively indicating favorable adsorption of arsenite onto those two adsorbents [41].

D–R model was used to calculate the sorption energy. D–R linear form can be applied to both homogeneous

Table 3
Pseudo-first-order and pseudo-second-order adsorption rate constants and calculated $q_{e,cal}$ and experimental $q_{e,exp}$ values for the adsorption of As(III) ions on BC and BC-CuO-NC. Initial metal ions concentration 77 mg/L; pH = 6.5; adsorbent dosage 0.35 g/50 mL; temperature 25°C

System	As(III)/BC	As(III)/BC-CuO-NC
$q_{e,exp}$ (mg/g)	22.831	36.765
Pseudo-first-order		
$q_{e,cal}$ (mg/g)	4.702	7.089
k_1 (1/min)	0.038	0.027
R^2	0.7489	0.7782
χ^2	29.622	33.624
$F_{error\%}$	55.59	45.43
Pseudo-second-order		
$q_{e,cal}$ (mg/g)	21.989	35.971
k_2 (g/mg min)	0.027	0.014
R^2	0.9997	0.9978
χ^2	0.055	0.078
$F_{error\%}$	1.71	1.67
Intraparticle diffusion equation		
k_{id}	0.414	0.663
C	18.226	28.177
R^2	0.8956	0.8891
χ^2	2.191	2.601
$F_{error\%}$	10.99	9.51

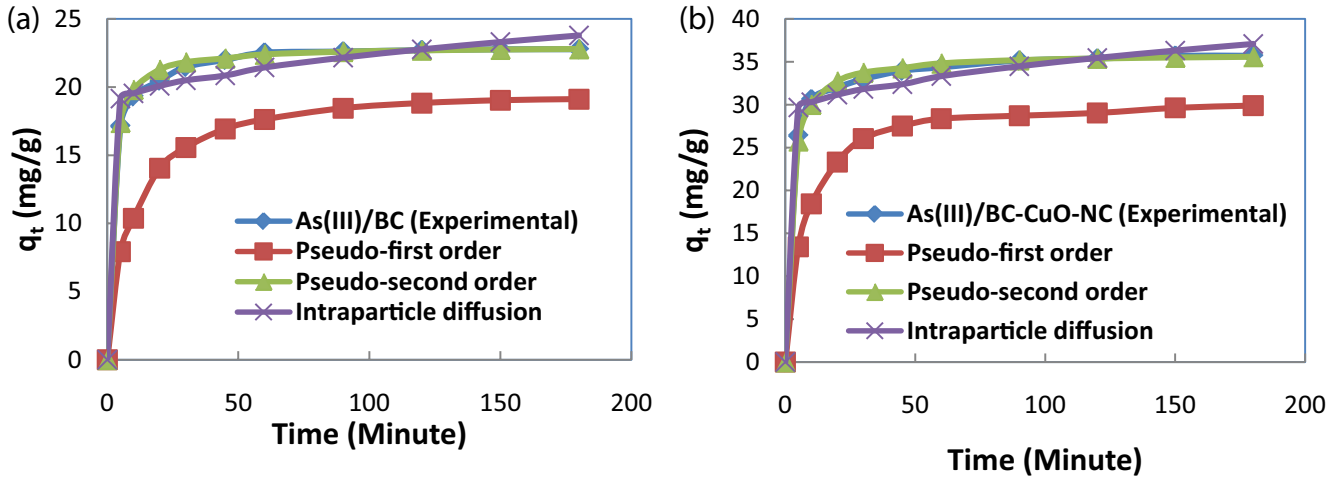

Fig. 8. Kinetic models for the adsorption of As(III) ions onto BC and BC-CuO-NC, using the nonlinear regression method. Initial metal ions concentration 77 mg/L; pH = 5.0; adsorbent dosage 0.35 g/50 mL; temperature 25°C.

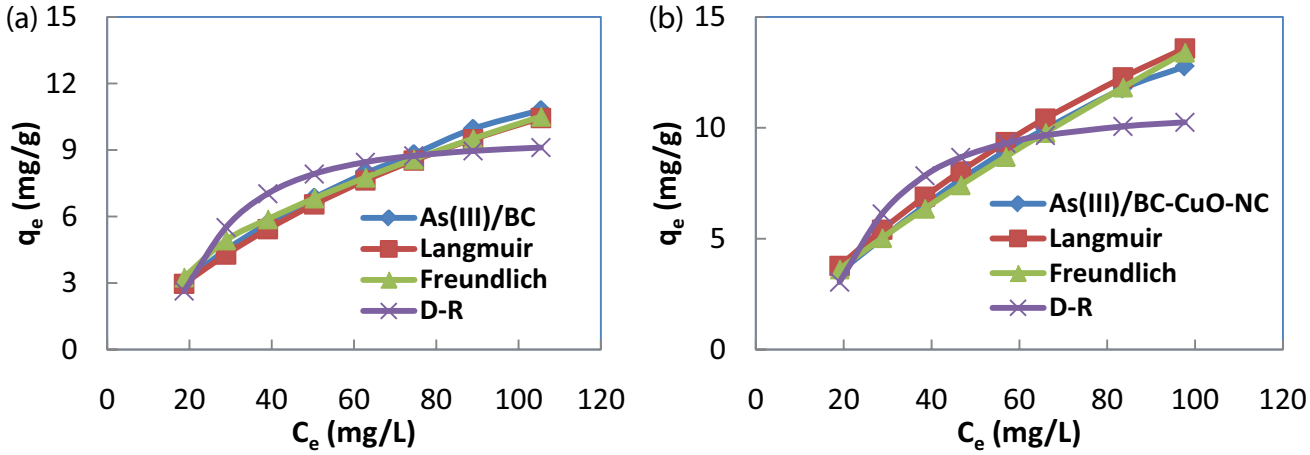

Fig. 9. Equilibrium isotherm for adsorption of As(III) ions onto BC and BC-CuO-NC, using the nonlinear regression method. Initial metal ions concentration 39–194 mg/L; pH = 6.5; adsorbent dosage 0.35 g/50 mL; temperature 25°C.

Table 4
Langmuir, Freundlich, and Dubinin–Radushkevich isotherm constants for the adsorption of As(III) ions on BC and BC-CuO-NC. Initial metal ions concentration 39–194 mg/L; pH = 6.5; adsorbent dosage 0.35 g/50 mL; temperature 25°C

Isotherm model	Parameter	BC	BC-CuO-NC
Langmuir	q_{max} (mg/g)	22.831	36.765
	K_L (L/mg)	0.008	0.006
	R_L	0.542	0.642
	R^2	0.9882	0.9778
	χ^2	0.097	0.195
	$F_{error\%}$	4.47	5.96
Freundlich	K_F (L/g)	0.413	0.343
	n	1.416	1.249
	R^2	0.9884	0.9923
	χ^2	0.098	0.056
	$F_{error\%}$	3.97	2.98
Dubinin–Radushkevich	q_{max} (mg/g)	9.505	10.780
	E (kJ/mol)	0.807	0.797
	R^2	0.7593	0.7564
	χ^2	1.525	1.539
	$F_{error\%}$	17.29	16.41

and heterogeneous surfaces [36]. Adsorption capacities q_{max} and adsorption free energy (E) are calculated and listed in Table 3. According to the literature [42] the adsorption is driven by physical forces if the value of E is less than 8 (kJ/mol), and driven by chemical ion-exchange if E is between 8 and 16 (kJ/mol), and driven by particle diffusion if the value of E is greater than 16 (kJ/mol). The results at all the experimental E values ranged between 0.061–0.077 kJ/mol for arsenite adsorption onto BC and E value ranged between 0.073–0.093 kJ/mol for arsenite adsorption onto BC-CuO-NC demonstrated the physical adsorption of arsenite onto BC, and BC-CuO-NC models surface. The possible adsorption interactions and pathways of the arsenite on BC and BC-CuO-NC surfaces could occur through electrostatic attractions and hydrogen bonding to BC and BC-CuO-NC phenolics. Thus, arsenite ions are adsorbed on the surface via interactions with functional groups, diffuse into the interior, and finally, achieve equilibrium in the adsorbent [43].

3.2.5. Thermodynamic parameter calculations

The adsorption thermodynamics was studied to gain an insight into the adsorption behaviors. Parameters including Gibbs free energy change ($\Delta G°$), enthalpy change ($\Delta H°$) and entropy change ($\Delta S°$) are calculated according to the following thermodynamic equations:

$$\Delta G° = -RT\ln K_d \tag{9}$$

K_d for the adsorption reaction can be defined [44]:

$$K_d = \frac{q_e}{C_e} \tag{10}$$

Values of K_d are obtained by plotting $\ln q_e/C_e$ vs. q_e and extrapolating q_e to zero.

$$\Delta G° = \Delta H° - T\Delta S° \tag{11}$$

$$\ln K_d = -\frac{\Delta H°}{RT} + \frac{\Delta S°}{R} \tag{12}$$

Predictions of the intercept and slope of the linear plot of $\ln K_d$ vs. $1/T$ (Fig. 10) give, respectively, $\Delta S°$ and $\Delta H°$ values. The values of thermodynamic parameters were summarized in Table 5. The obtained results showed that Gibbs energy ($\Delta G°$) was negative at the adsorption of arsenite onto BC and BC-CuO-NC model. This indicates that the adsorption processes of arsenite onto BC and BC-CuO-NC were spontaneous and can be enhanced by increasing temperature. The adsorption of the arsenite onto BC and BC-CuO-NC

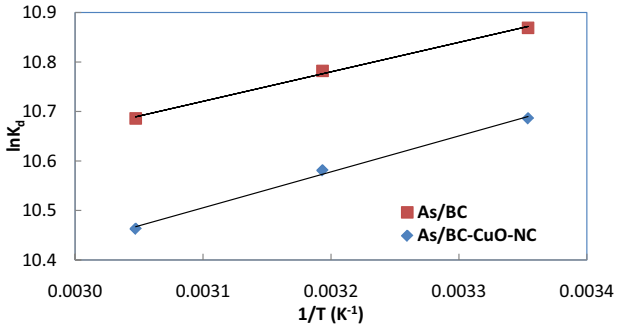

Fig. 10. Determination of $\Delta H°$ and $\Delta S°$ using the van't Hoff equation for the adsorption of As(III) ions onto BC and BC-CuO-NC.

Table 5
Thermodynamic parameters for the adsorption of arsenite onto BC and BC-CuO-NC

T/K	lnK_d	$\Delta G°$ (kJ/mol)	$\Delta H°$ (kJ/mol)	$\Delta S°$ (J/K mol)
As(III)/BC				
298.15	10.819	–26.820		
313.15	10.732	–27.943	–4.947	73.163
328.15	10.636	–29.019		
As(III)/BC-CuO-NC				
298.15	10.636	–26.366		
313.15	10.531	–27.419	–6.036	68.175
328.15	10.413	–28.411		

is physisorption because $\Delta G°$ for physisorption is between –40 and 0 kJ/mol. The negative values of $\Delta H°$ mean that the adsorption process is exothermic. In an exothermic process, the total energy absorbed in bond breaking is less than the total energy released in the bond making between adsorbate and adsorbent, resulting in the absorbing of energy in the form of heat. The standard entropy change ($\Delta S°$) for arsenite adsorbed onto BC and BC-CuO-NC was positive. This positive $\Delta S°$ value showed the increased disorder and randomness at the solid-solution interface.

4. Conclusions

In this study, Mediterranean cypress cones and its aqueous extract have been used as a green synthesis of CuO-NP's, BC, and BC-CuO-NC. Adsorption of As(III) from an aqueous solution was investigated using BC and BC-CuO-NC as an adsorbent. Based on R^2, χ^2 and $F_{error\%}$ values, the results of adsorption isotherms and kinetics suggested that both Langmuir and Freundlich models and the pseudo-second-order model were best to model the As(III) adsorption onto BC and BC-CuO-NC. The maximum adsorption q_{max} of As(III) onto BC, and BC-CuO-NC was found to be 22.831, and 36.765 mg/g respectively. Thermodynamic parameters $\Delta G°$, $\Delta H°$, and, $\Delta S°$ showed the exothermic and spontaneous nature of the adsorption of As(III) onto BC and BC-CuO-NC. Finally, the BC-CuO-NC might be employed as a promising material and future solution for the removal of As(III) for a clean environment.

Acknowledgment

The author would like to thank the Deanship of Scientific Research at the University of Jordan for supporting the idea of this study.

References

[1] J. Alchouron, C. Navarathna, P.M. Rodrigo, A. Snyder, H.D. Chludil, A.S. Vega, G. Bosi, F. Perez, D. Mohan, C.U. Pittman Jr., T.E. Mlsna, Household arsenic contaminated water treatment employing iron oxide/bamboo biochar composite: an approach to technology transfer, J. Colloid Interface Sci., 587 (2021) 767–779.
[2] R. Singh, S. Singh, P. Parihar, V.P. Singh, S.M. Prasad, Arsenic contamination, consequences and remediation techniques: a review, Ecotoxicol. Environ. Saf., 112 (2015) 247–270.
[3] P. Chutia, S. Kato, T. Kojima, S. Satokawa, Arsenic adsorption from aqueous solution on synthetic zeolites, J. Hazard. Mater., 162 (2009) 440–447.
[4] F.W. Pontius, K.G. Brown, C.J. Chen, Health implications of arsenic in drinking water, J. Am. Water Works Assn., 86 (1994) 52–63.
[5] A.A. Meharg, J. Hartley-Whitaker, Arsenic uptake and metabolism in arsenic resistant and nonresistant plant species, New Phytol., 154 (2002) 29–43.
[6] D. Vromman, J.-P. Martínez, M. Kumar, Z. Šlejkovec, S. Lutts, Comparative effects of arsenite (As(III)) and arsenate (As(V)) on whole plants and cell lines of the arsenic-resistant halophyte plant species *Atriplex atacamensis*, Environ. Sci. Pollut. Res., 25 (2018) 34473–34486.
[7] C.M. George, L. Sima, M.H.J. Arias, J. Mihalic, L.Z. Cabrera, D. Danz, W. Checkley, R.H. Gilman, Arsenic exposure in drinking water: an unrecognized health threat in Peru, Bull. World Health Organ., 92 (2014) 565–572.
[8] C.-C. Chen, Y.-C. Chung, Arsenic removal using a biopolymer chitosan sorbent, J. Environ. Sci. Health. Part A Toxic/Hazard. Subst. Environ. Eng., 41 (2006) 645–658.
[9] J. Alchouron, C. Navarathna, H.D. Chludil, N.B. Dewage, F. Perez, E.B. Hassan, C.U. Pittman Jr., A.S. Vega, T.E. Mlsna, Assessing South American *Guadua chacoensis* bamboo biochar and Fe_3O_4 nanoparticle dispersed analogues for aqueous arsenic(V) remediation, Sci. Total Environ., 706 (2020) 135943, https://doi.org/10.1016/j.scitotenv.2019.135943.
[10] H. Rasheed, P. Kay, R. Slack, Y.Y. Gong, A. Carter, Human exposure assessment of different arsenic species in household water sources in a high risk arsenic area, Sci. Total Environ., 584–585 (2017) 631–641.
[11] L. Singh, P. Semil, Removal of arsenic in aqueous solution by low cost adsorbent: a short review, Int. J. ChemTech Res., 5 (2013) 1299–1308.
[12] N.V. Vinh, M. Zafar, S.K. Behera, H.-S. Park, Arsenic(III) removal from aqueous solution by raw and zinc-loaded pine cone biochar: equilibrium, kinetics, and thermodynamics studies, Int. J. Environ. Sci. Technol., 12 (2014) 1283–1294.
[13] D. Mohan, C.U. Pittman Jr., Arsenic removal from water/wastewater using adsorbents—a critical review, J. Hazard. Mater., 142 (2007) 1–53.
[14] R. Kumar, M. Patel, P. Singh, J. Bundschuh, C.U. Pittman Jr., L. Trakal, D. Mohan, Emerging technologies for arsenic removal from drinking water in rural and peri-urban areas: methods, experience from, and options for Latin America, Sci. Total Environ., 694 (2019) 133427, https://doi.org/10.1016/j.scitotenv.2019.07.233.
[15] C.M. Navarathna, N.B. Dewage, C. Keeton, J. Pennisson, R. Henderson, B. Lashley, X.F. Zhang, E.B. Hassan, F. Perez, D. Mohan, C.U. Pittman Jr., T. Mlsna, Biochar adsorbents with

enhanced hydrophobicity for oil spill removal, ACS Appl. Mater. Interfaces, 12 (2020) 9248–9260.
[16] X.-f. Tan, Y.-g. Liu, Y.-l. Gu, Y. Xu, G.-m. Zeng, X.-j. Hu, S.-b. Liu, X. Wang, S.-m. Liu, J. Li, Biochar-based nano-composites for the decontamination of wastewater: a review, Bioresour. Technol., 212 (2016) 318–333.
[17] D. Borah, S. Satokawa, S. Kato, T. Kojima, Surface-modified carbon black for As(V) removal, J. Colloid Interface Sci., 319 (2008) 53–62.
[18] J.W. Kim, J.Y. Song, S.-M. Lee, J.H. Jung, Application of iron-modified biochar for arsenite removal and toxicity reduction, J. Ind. Eng. Chem., 80 (2019) 17–22.
[19] K.Z. Benis, A.M. Damuchali, J. Soltan, K.N. McPhedran, Treatment of aqueous arsenic – a review of biochar modification methods, Sci. Total Environ., 739 (2020) 139750, https://doi.org/10.1016/j.scitotenv.2020.139750.
[20] C.M. Navarathna, A.G. Karunanayake, S.R. Gunatilake, C.U. Pittman Jr., F. Perez, D. Mohan, T. Mlsna, Removal of Arsenic(III) from water using magnetite precipitated onto Douglas fir biochar, J. Environ. Manage., 250 (2019) 109429, https://doi.org/10.1016/j.jenvman.2019.109429.
[21] A. El Hanandeh, R.A. Abu-Zurayk, I. Hamadneh, A.H. Al-Dujaili, Characterization of biochar prepared from slow pyrolysis of Jordanian olive oil processing solid waste and adsorption efficiency of Hg^{2+} ions in aqueous solutions, Water Sci. Technol., 74 (2016) 1899–1910.
[22] J.-Q. Jiang, S.M. Ashekuzzaman, J.S.J. Hargreaves, A.R. McFarlane, A.B.M. Badruzzaman, M.H. Tarek, Removal of arsenic(III) from groundwater applying a reusable Mg-Fe-Cl layered double hydroxide, J. Chem. Technol. Biotechnol., 90 (2015) 1160–1166.
[23] C.H. Chia, B. Gong, S.D. Joseph, C.E. Marjo, P. Munroe, A.M. Rich, Imaging of mineral-enriched biochar by FTIR, Raman and SEM–EDX, Vib. Spectrosc., 62 (2012) 248–257.
[24] P.C. Nagajyothi, P. Muthuraman, T.V.M. Sreekanth, D.H. Kim, J. Shim, Green synthesis: *in-vitro* anticancer activity of copper oxide nanoparticles against human cervical carcinoma cells, Arabian J. Chem., 10 (2017) 215–225.
[25] H.P. Yang, R. Yan, H.P. Chen, D.H. Lee, C. Zheng, Characteristics of hemicellulose, cellulose and lignin pyrolysis, Fuel, 86 (2007) 1781–1788.
[26] S.X. Tan, W.J. Zou, F.P. Jiang, S.Z. Tan, Y.L. Liu, D.S. Yuan, Facile fabrication of copper-supported ordered mesoporous carbon for antibacterial behavior, Mater. Lett., 64 (2010) 2163–2166.
[27] A.D. Igalavithana, Y.S. Ok, N.K. Niazi, M. Rizwan, M.I. Al-Wabel, A.R.A. Usman, D.H. Moon, S.S. Lee, Effect of corn residue biochar on the hydraulic properties of sandy loam soil, Sustainability, 9 (2017) 266, https://doi.org/10.3390/su9020266.
[28] M. Nasrollahzadeh, M. Maham, S. Mohammad Sajadi, Green synthesis of CuO nanoparticles by aqueous extract of *Gundelia tournefortii* and evaluation of their catalytic activity for the synthesis of *N*-monosubstituted ureas and reduction of 4-nitrophenol, J. Colloid Interface Sci., 455 (2015) 245–253.
[29] S.N. do Carmo Ramos, A.L.P. Xavier, F.S. Teodoro, L.F. Gil, L.V.A. Gurgel, Removal of cobalt(II), copper(II), and nickel(II) ions from aqueous solutions using phthalate-functionalized sugarcane bagasse: mono- and multicomponent adsorption in batch mode, Ind. Crops Prod., 79 (2016) 116–130.
[30] M.B. Ahmed, J.L. Zhou, H.H. Ngo, W.S. Guo, M.F. Chen, Progress in the preparation and application of modified biochar for improved contaminant removal from water and wastewater, Bioresour. Technol., 214 (2016) 836–851.
[31] B. Liang, J. Lehmann, D. Solomon, J. Kinyangi, J. Grossman, B. O'Neill, J.O. Skjemstad, J. Thies, F.J. Luizão, J. Petersen, E.G. Neves, Black carbon increases cation exchange capacity in soils, Soil Sci. Soc. Am. J., 70 (2006) 1719–1730.
[32] M. Ishaq, S. Sultan, I. Ahmad, H. Ullah, M. Yaseen, A. Amir, Adsorptive desulfurization of model oil using untreated, acid activated and magnetite nanoparticle loaded bentonite as adsorbent, J. Saudi Chem. Soc., 21 (2017) 143–151.
[33] S. Lagergren, About the theory of so-called adsorption of soluble substances, Kungliga Svenska Vetenskapsakademiens Handlingar, 24 (1898) 1–39.
[34] Y.-S. Ho, Review of second-order models for adsorption systems, J. Hazard. Mater., 36 (2006) 681–689.
[35] W.J. Weber, J.C. Morris, Kinetics of adsorption on carbon from solution, J. Sanit. Eng. Div., 89 (1963) 31–60.
[36] N.A.S. Mohammed, R.A. Abu-Zurayk, I. Hamadneh, A.H. Al-Dujaili, Phenol adsorption on biochar prepared from the pine fruit shells: equilibrium, kinetic and thermodynamics studies, J. Environ. Manage., 226 (2018) 377–385.
[37] G. Yang, H.L. Chen, H.D. Qin, Y.J. Feng, Amination of activated carbon for enhancing phenol adsorption: effect of nitrogen-containing functional groups, Appl. Surf. Sci., 293 (2014) 299–305.
[38] I. Langmuir, The adsorption of gases on plane surfaces of glass, mica and platinum, J. Am. Chem. Soc., 40 (1918) 1361–1403.
[39] H.M.F. Freundlich, About the adsorption, Zeitschrift für Physikalische Chemie, 57 (1906) 385–470.
[40] M.M. Dubinin, E.D. Zaverina, L.V. Radushkevich, Sorption and structure of active carbon I. Adsorption of organic vapors, J. Phys. Chem. A, 21 (1947) 1351–1362.
[41] D. Hsu, C.Y. Lu, T.R. Pang, Y.P. Wang, G.H. Wang, Adsorption of ammonium nitrogen from aqueous solution on chemically activated biochar prepared from sorghum distillers grain, Appl. Sci. (Switzerland), 9 (2019) 5249, https://doi.org/10.3390/app9235249.
[42] H. Chen, J. Zhao, G.L. Dai, J.Y. Wu, H. Yan, Adsorption characteristics of Pb(II) from aqueous solution onto a natural biosorbent, fallen *Cinnamomum camphora* leaves, Desalination, 262 (2010) 174–182.
[43] Z.H. Yu, L. Zhou, Y.F. Huang, Z.G. Song, W.W. Qiu, Effects of a manganese oxide-modified biochar composite on adsorption of arsenic in red soil, J. Environ. Manage., 163 (2015) 155–162.
[44] H.N. Tran, S.-J. You, A. Hosseini-Bandegharaei, H.-P. Chao, Mistakes and inconsistencies regarding adsorption of contaminants from aqueous solutions: a critical review, Water Res., 120 (2017) 88–116.